Journal of Biomedical Optics

BiomedicalOptics.SPIEDigitalLibrary.org

Wearable near-infrared optical probe for continuous monitoring during breast cancer neoadjuvant chemotherapy infusions

Fei Teng
Timothy Cormier
Alexis Sauer-Budge
Rachita Chaudhury
Vivian Pera
Raeef Istfan
David Chargin
Samuel Brookfield
Naomi Yu Ko
Darren M. Roblyer

SPIE.

Fei Teng, Timothy Cormier, Alexis Sauer-Budge, Rachita Chaudhury, Vivian Pera, Raeef Istfan, David Chargin, Samuel Brookfield, Naomi Yu Ko, Darren M. Roblyer, "Wearable near-infrared optical probe for continuous monitoring during breast cancer neoadjuvant chemotherapy infusions," *J. Biomed. Opt.* **22**(1), 014001 (2017), doi: 10.1117/1.JBO.22.1.014001.

Wearable near-infrared optical probe for continuous monitoring during breast cancer neoadjuvant chemotherapy infusions

Fei Teng,[a] Timothy Cormier,[b] Alexis Sauer-Budge,[b] Rachita Chaudhury,[c] Vivian Pera,[c] Raeef Istfan,[c] David Chargin,[b] Samuel Brookfield,[b] Naomi Yu Ko,[d] and Darren M. Roblyer[c,*]
[a]Boston University, Department of Electrical and Computer Engineering and Photonics Center, 8 Saint Mary's Street, Boston, Massachusetts 02215, United States
[b]Boston University, Fraunhofer Center for Manufacturing Innovation, 15 Saint Mary's Street, Brookline, Massachusetts 02446, United States
[c]Boston University, Department of Biomedical Engineering, 44 Cummington Mall, Boston, Massachusetts 02215, United States
[d]Boston Medical Center, Section of Hematology and Oncology, Women's Health Unit, 801 Massachusetts Avenue, First Floor, Boston, Massachusetts 02118, United States

Abstract. We present a new continuous-wave wearable diffuse optical probe aimed at investigating the hemodynamic response of locally advanced breast cancer patients during neoadjuvant chemotherapy infusions. The system consists of a flexible printed circuit board that supports an array of six dual wavelength surface-mount LED and photodiode pairs. The probe is encased in a soft silicone housing that conforms to natural breast shape. Probe performance was evaluated using tissue-simulating phantoms and *in vivo* normal volunteer measurements. High SNR (71 dB), low source-detector crosstalk (−60 dB), high measurement precision (0.17%), and good thermal stability (0.22% V_{rms}/°C) were achieved in phantom studies. A cuff occlusion experiment was performed on the forearm of a healthy volunteer to demonstrate the ability to track rapid hemodynamic changes. Proof-of-principle normal volunteer measurements were taken to demonstrate the ability to collect continuous *in vivo* breast measurements. This wearable probe is a first of its kind tool to explore prognostic hemodynamic changes during chemotherapy in breast cancer patients. © *The Authors. Published by SPIE under a Creative Commons Attribution 3.0 Unported License. Distribution or reproduction of this work in whole or in part requires full attribution of the original publication, including its DOI.* [DOI: 10.1117/1.JBO.22.1.014001]

Keywords: continuous-wave diffuse optical imaging; wearables; tissue hemodynamics.

Paper 160728SSPR received Oct. 21, 2016; accepted for publication Dec. 21, 2016; published online Jan. 13, 2017.

1 Introduction

Optical wearables may provide new opportunities for tracking healthy and disease states longitudinally, including time points currently unobtainable with standard-of-care clinical imaging modalities. Superficial-probing wearable optical heart rate monitors are widely available in the consumer space for fitness tracking, but there has been substantially less development in the medical space for deep tissue applications in oncology. We present here a new diffuse optical wearable probe, designed to track tumor metabolism and hemodynamic changes during breast cancer chemotherapy treatment. This new imaging platform may allow for the identification of important new prognostic timepoints that can be used to modify treatment and drug regimens for individual patients.

The optical measurement of tumors in the breast typically requires the measurement of multiply scattered near-infrared (NIR) light, which has traveled up to several centimeters in depth. Due to the diffusive nature of photon propagation in thick biological tissue, techniques that employ these measurements are usually referred to as diffuse optical imaging (DOI) or diffuse optical spectroscopy (DOS).[1] These methods have been widely shown to be capable of extracting tissue level concentrations and/or changes in concentration of key functional parameters in the breast, brain, muscle, and other tissues. Depending on wavelengths utilized, the parameters may include oxyhemoglobin, deoxyhemoglobin, water, and lipids.[2] Diffuse optical techniques can be broadly classified into three variants: continuous-wave (CW), frequency-domain (FD), and time-domain (TD) methods. FD and TD techniques provide separation of optical absorption and scattering effects but typically require modulated or pulsed laser sources and sensitive avalanche photodiodes or photomultiplier tube detectors.[3–5] CW techniques can provide relative changes in tissue chromophores if assumptions or prior knowledge of the wavelength dependence of scattering are available.[6] In situations in which the optical scattering can be assumed to be time-invariant, CW DOI or DOS can be used to monitor hemodynamic and metabolic changes in tissue with relatively simple instrumentation and analysis techniques. This is especially relevant over short time periods (seconds to hours).[7–9] Measurements are possible with inexpensive LEDs and photodiodes, and surface-mount packaging of these components reduces the device footprint and facilitates the design of flexible optical probes that can be used in direct contact with skin. These features provide the possibility for wearable CW imaging probes for measurements of deep tissue hemodynamics. Several optical wearables have been previously developed and applied for studies related to cardiology,[10] general purpose blood oxygen saturation,[10,11] and cerebral activity,[11–15] but we know of no prior work in optical wearables for tumor chemotherapy monitoring.

Prior DOI and DOS instrumentation, which include both largely immobile platforms and more portable handheld probes,

*Address all correspondence to: Darren M. Roblyer, E-mail: roblyer@bu.edu

have been previously utilized to monitor chemotherapy response in breast cancer patients receiving neoadjuvant (presurgical) chemotherapy. FD techniques,[16–21] TD techniques,[22–25] and CW techniques[26–28] have been employed to track tumor hemoglobin, water, and lipid changes throughout treatment. Most prior studies have been focused on changes in tissue chromophore concentrations after weeks of treatment. For example, Cerussi et al. showed that by comparing the functional properties between tumor and normal tissue, breast cancer patients who achieved pathologic complete response to neoadjuvant chemotherapy had a 23% reduction in total hemoglobin on average by the midpoint in treatment compared to an 11% reduction in partial and nonresponders.[29] Other groups have shown similar trends.[18,30–32] Recently, it was reported that changes in oxyhemoglobin concentration on the first day after an initial chemotherapy infusion could statistically differentiate responders from nonresponders.[20] We hypothesize that hemodynamic changes during the first chemotherapy infusion (typically lasting several hours) may also be prognostic of long-term treatment response. A new wearable CW DOI probe is presented here, which was designed to monitor these very early time points. The performance of the probe was evaluated *in vitro* using tissue-simulating phantoms and *in vivo* with a cuff occlusion test. Additionally, a normal volunteer was measured continuously over a period of 10 min to evaluate the stability and comfort of the probe.

2 Instrument Design

The CW wearable probe was designed to be flexible in order to accommodate the natural curvature of human breast tissue. Figure 1(a) shows the flexible printed circuit board (PCB) with optical and electrical components. The flexible PCB was fabricated with two mil (51 μm) copper and polyimide. From the central hub of the wearable probe, six flexible arms radiate and form into the backbone of a hexagon. Each arm has an LED pair at its terminal end; the seventh arm terminates with a micro-HDMI connector. A photodiode module is positioned at the central hub.

The surface mount LED pairs (SMT750-23 and SMT850-23, Roithner Lasertechnik) have a peak emission wavelength of 750 and 850 nm, and each generates a total optical output power of ~20 mW at a 50-mA forward current.[33] The optical detector module (TSL250RD, ams AG) has a 1-mm active area photodiode with an integrated transimpedance amplifier with an irradiance responsivity of ~74 $\mathrm{mV}/(\mu\mathrm{W}/\mathrm{cm}^2)$. The source–detector separation between the LEDs and the photodiode is 25.4 mm. Similar source–detector separations have been shown to provide adequate optical depth penetration for measurements of most breast tumors eligible for neoadjuvant chemotherapy.[8,20,34,35] A thin plastic stiffener was fabricated to add rigidity from the central hub to the seventh radiating arm, which serves as the cable connection point. A 19-pin micro HDMI cable is used to communicate between the wearable probe and benchtop control electronics. Figures 1(b) and 1(c) show the completed probe. A hexagonal medical grade silicone housing encapsulates the probe and has a dimension of 90.7 mm between the opposite vertices. The maximum thickness of the encapsulated probe is 11.3 mm, and it has a total mass of 48.9 g. The probe is highly flexible along all dimensions except

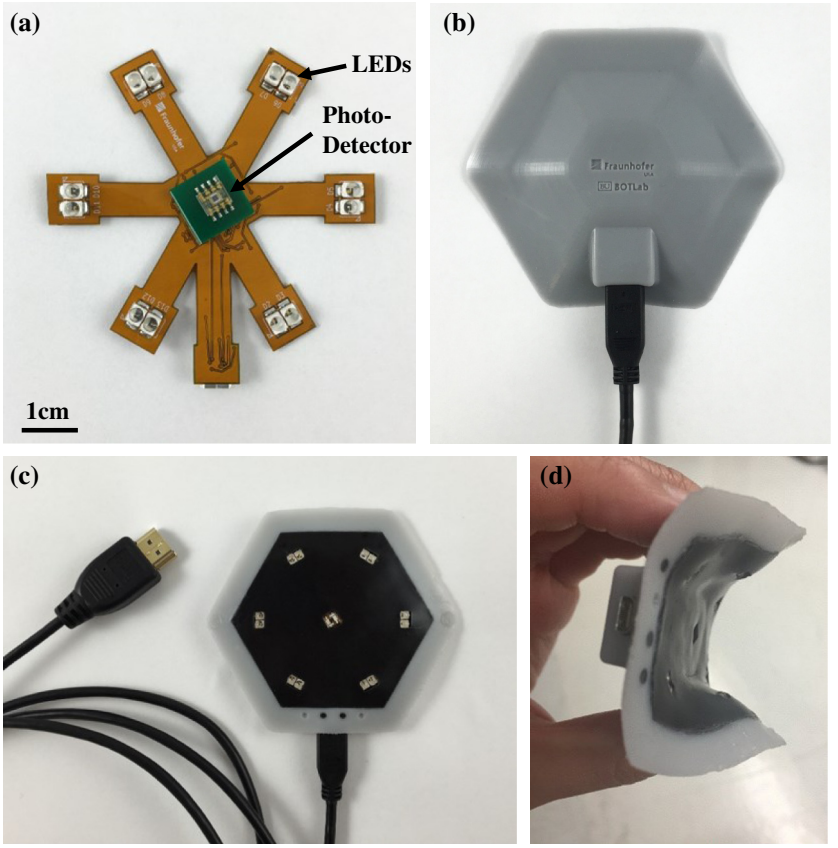

Fig. 1 (a) Flexible PCB and optical components. (b) Top and (c) bottom view of the wearable probe. (d) Flexibility of the probe under gentle pressure.

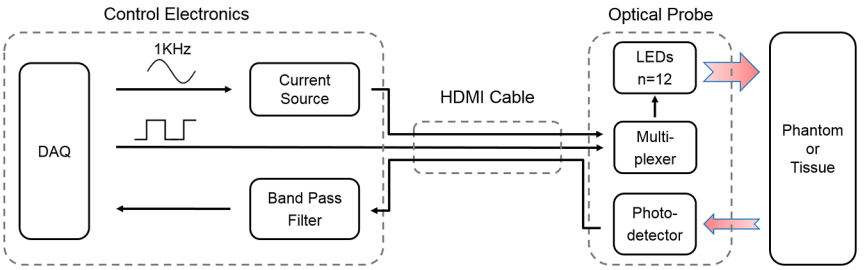

Fig. 2 Schematic view of CW DOI system. Solid line: electrical signal. Red arrow: optical signal.

the dimension parallel to the HDMI cable due to the plastic stiffener [Fig. 1(d)].

Figure 2 shows a block diagram of the probe and control electronics. A data acquisition board (National Instruments USB-6361) provides a low frequency sinusoidal analog signal as a modulation input to the current controller (ILX Lightwave, LDX-3525B), which in turn provides the forward current to the LEDs with a modulation index of 0.9. The forward current is modulated at 1 KHz to assist in rejection of background noise, 60 Hz electrical noise and harmonics, and to match the response from the photodetector. A 4-bit digital control signal is also generated by the DAQ to control the sequence of LED illumination. Digital and analog signals are delivered to the probe through an HDMI cable. The digital lines are fed into a 4-to-16 line decoder (74HC/HCT4514, Philips Semiconductors), which direct the current into individual LEDs through a bank of MOSFET switches. On the detection side, the photodiode provides a linear response to light intensity, and photocurrent is converted to a voltage signal with an integrated transimpedance amplifier. The amplified signal is routed through the HDMI cable and is further amplified by 10 dB and filtered through a custom 1 KHz eighth order Bessel band-pass filter (BPF) with a 200 Hz, −3 dB passband width prior to data acquisition. The probe is controlled using a custom LabView program.

During operation, each of the 12 LEDs is illuminated sequentially, and a complete measurement cycle is defined as measurements collected from all 12 optode pairs. Data are acquired at 100 K samples/s with a sampling length of 50 ms for each optode. Due to the delay from BPF settling time, and other optical and electronic components, a 35-ms delay was added between optode measurements. A complete measurement cycle takes 1020 ms (85 ms × 12). A delay can be added between measurement cycles depending on desired experimental conditions.

3 Instrument Performance

Initial performance testing was conducted using tissue simulating silicone solid phantoms and blood–intralipid based liquid phantoms.

3.1 *Signal-to-Noise Ratio, Dynamic Range, and System Crosstalk*

The system voltage outputs were processed using a fast Fourier transform (FFT) with a rectangular window to compute SNR and dynamic range. Power measurements of the signal-of-interest were summed over a 500-Hz band centered at 1 KHz in the FFT, and DC and the first 10 harmonics were excluded for these calculations. SNR and dynamic range were calculated as $10\log(P_{\text{signal}}/P_{\text{noise}})$. SNR measurements were taken on a set of three breast-like tissue-simulating solid phantoms with the following optical properties: phantom 1: $\mu_a = 0.0054$ mm^{-1} (750 nm), $\mu_a = 0.0038$ mm^{-1} (850 nm), $\mu_s' = 1.2$ mm^{-1} (750 nm), $\mu_s' = 1.0$ mm^{-1} (850 nm); phantom 2: $\mu_a = 0.0045$ mm^{-1} (750 nm), $\mu_a = 0.0032$ mm^{-1} (850 nm), $\mu_s' = 1.1$ mm^{-1} (750 nm), $\mu_s' = 0.9$ mm^{-1} (850 nm); phantom 3: $\mu_a = 0.0036$ mm^{-1} (750 nm), $\mu_a = 0.0026$ mm^{-1} (850 nm), $\mu_s' = 0.9$ mm^{-1} (750 nm), $\mu_s' = 0.8$ mm^{-1} (850 nm). These optical properties closely match prior reported normal breast tissue values.[36,37] A SNR >68 dB for channels with 750-nm LEDs and >71 dB for channels with 850-nm LEDs was achieved for measurement on a breast-like tissue-simulating solid phantom. The system dynamic range was at least 80.4 dB when measuring the maximum optical signal level. During normal operation, it is possible that light may travel directly from source to detector along the tissue surface causing undesired optical source–detector crosstalk. Additionally, inductive coupling may cause undesired electrical crosstalk at the PCB level or in the HDMI cable. In order to evaluate both electrical and optical crosstalk, measurements were taken on a highly absorbing black phantom, and a 7-dB signal for the 750-nm LEDs and 6-dB signal for 850-nm LEDs were observed at the 1-KHz modulation frequency relative to the average noise floor. This indicates that the crosstalk signal is at least 60 dB weaker than the signal from breast-like tissue phantom measurements.

3.2 *System Drift*

A system drift test was performed to evaluate the repeatability of the system under static experimental conditions. About 180 repeat measurement cycles were acquired over 90 min (a typical chemotherapy infusion length), and results from each source–detector (optode) pair were normalized relative to the root-mean-square value of modulated signal (V_{rms}) from the first measurement. Figure 3 shows the drift for each source–detector pair (each source–detector pair is identified by its probe arm in the figure legend). On average, an absolute system precision of 0.17% was achieved for optical channels with 750-nm LEDs and a precision of 0.18% was achieved for optical channels with 850-nm LEDs. The largest single optode drift was observed in probe arm 4, equaling 0.40% and 0.51% for the 750-nm and 850-nm LEDs, respectively. These results indicate that the probe is capable of highly repeatable measurements.

3.3 *Thermal Stability*

A thermal stability test was conducted in order to determine the sensitivity of the probe to different ambient temperatures. This is relevant as the probe will be placed directly against the subject's skin, and skin temperature may change over time. A thermal sensor from a thermal data logger was positioned in contact

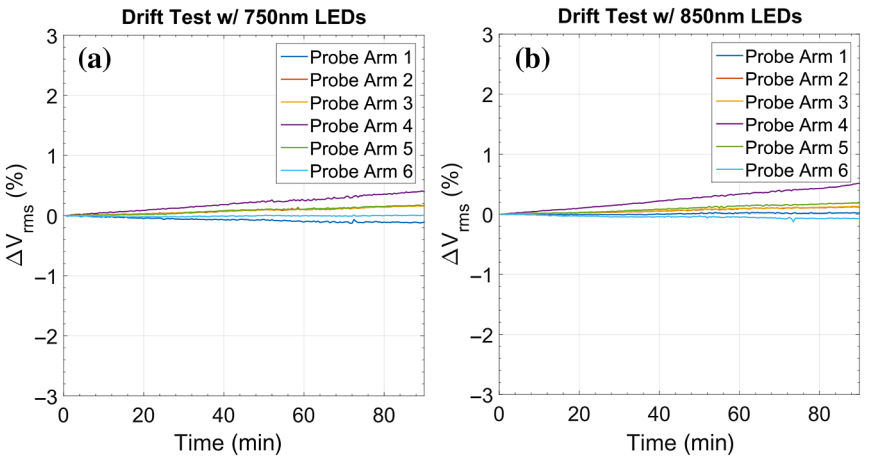

Fig. 3 System drift test. Results are shown for (a) the 750-nm and (b) 850-nm optical channels. An average drift of 0.18% or less was observed over the 90-min test.

with the underside of the probe. Five minutes of repeated measurements were taken on a solid phantom to establish a baseline; measurements were taken every 5 s. The local temperature of the probe was controlled using a hotplate, which was positioned under the optical phantom. The hotplate was then turned on and the probe temperature rose from ~26.6°C to 39.2°C over a period of ~14 min. Figure 4 shows the thermal response of the probe for the 750-nm and 850-nm optical channels. Within a normal physiological temperature range[38] (indicated by the area between two horizontal dashed lines in Fig. 4), measured voltage changes correspond to an average thermal response of 0.35% V_{rms}/deg (V_{rms}/°C) for the 750-nm channels and 0.22% V_{rms}/deg (V_{rms}/°C) for the 850-nm channels. These results indicate only minor fluctuations in instrument response over the expected operating temperature range.

3.4 *Probe Accuracy*

To determine the accuracy of the wearable probe, it was tested against a commercial dissolved oxygen (DO) sensor (VisiFerm DO Arc 120, Hamilton Robotics), which served as a gold standard for this study. Measurements were taken on a blood–intralipid based liquid phantom during dynamic oxygenation changes. The phantom was made by adding 17 ml of pooled bovine blood (Carolina Biological Supply Company), 48 ml of intralipid (Fresenius Kabi, 20% I.V. Fat Emulsion), 120 ml of 10× phosphate-buffered saline solution (Fisher Scientific), and 1015 ml of deionized water for a total phantom volume of 1200 ml. The phantom was contained in a 6-in. diameter cylindrical baking pan placed on a stirring hotplate, which maintained a constant phantom temperature of 37°C. A magnetic stir bar was used to stir the phantom at a constant spinning rate of 120 revolutions/min.

The phantom started near 100% oxygen saturation and was slowly deoxygenated by adding a solution of baker's yeast, made by dissolving active dry yeast into deionized water with a concentration of 1 mg/ml. A total of 4.2-ml yeast solution was gradually added to the phantom, which caused a change in oxygen saturation from ~100% to 34% over a 43-min period. During this time, the wearable probe and the DO sensor simultaneously monitored the hemodynamics in the liquid phantom. Temperature and pH were monitored continuously throughout the test. The DO sensor measures the concentration of unbound oxygen, and DO concentrations were converted to oxygen saturation values using a published dissociation curve for matching temperature and pH levels.[39] DO measurements were taken every 5 s over the 43-min period.

The modified Beer–Lambert law (MBLL) was utilized to convert the raw V_{rms} measurements from the wearable probe to oxygen saturation values as well as changes in oxyhemoglobin and deoxyhemoglobin concentration.[40] Measurements of the

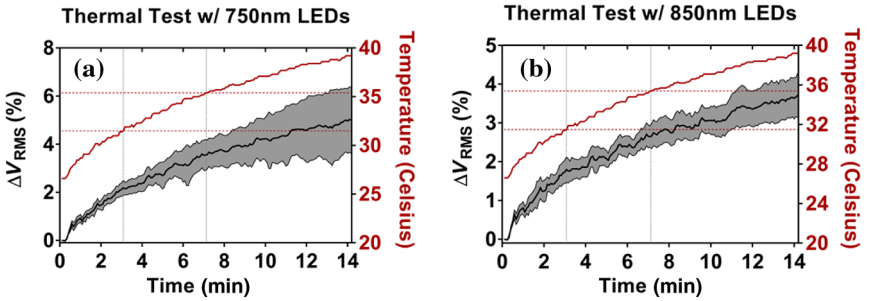

Fig. 4 System thermal response to local probe temperature changes. The red solid line corresponds to the local temperature measured at the probe, while the black solid line corresponds to the normalized changes in detector voltage levels. The shaded area indicates the standard derivation calculated from the optodes that share the same wavelength. The red dashed lines show the upper and lower bound of normal physiological temperature of human skin.[38] (a) Thermal test w/750 nm LEDs and (b) thermal test w/850 nm LEDs.

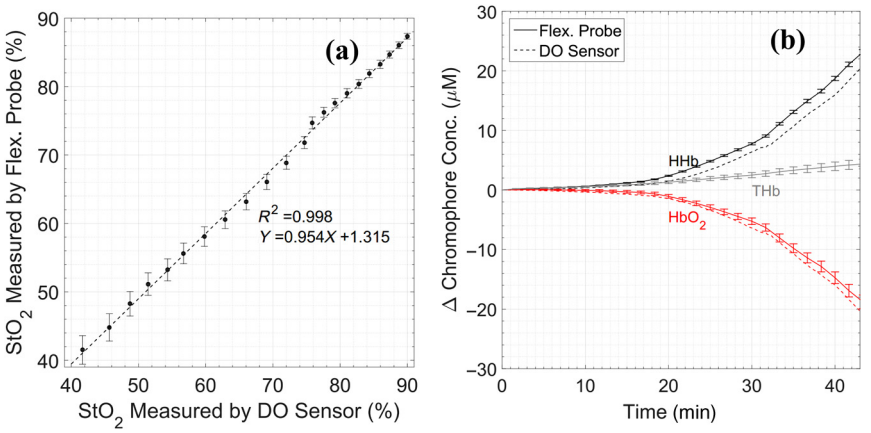

Fig. 5 Probe results compared to a DO sensor for (a) oxygen saturation and (b) chromophore concentration changes measurements taken from a blood–intralipid phantom during phantom deoxygenation.

initial optical properties of the liquid phantom were taken using an in-house FD diffuse optical spectroscopic imaging system. The initial optical properties were then used to calculate a differential pathlength factor assuming a homogeneous semi-infinite medium:[41]

$$\mathrm{DPF}(\lambda) = \frac{1}{2}\left[\frac{3\mu_s'(\lambda)}{\mu_a(\lambda)}\right]^{\frac{1}{2}}\left[1 - \frac{1}{(1 + d[3\mu_a(\lambda)\mu_s'(\lambda)]^{\frac{1}{2}}}\right], \quad (1)$$

where $\mu_a(\lambda)$ and $\mu_s'(\lambda)$ are the absorption and reduced scattering coefficient of diffusive medium, d is the separation of source and detector on the probe. The liquid phantom had a total hemoglobin concentration of ~30.8 μM, which is estimated from previously reported values for bovine blood (13 to 15 g/100 mL).[42] Changes from an initial value of ~100% oxygen saturation (as verified by the DO sensor) were computed and compared with values from the DO sensor. Wearable probe measurements were taken once every 5 s during the 43-min period.

Figure 5(a) shows the agreement between the wearable probe and the DO sensor for saturation values between 40% and 90%. Typical oxygen saturation levels of human breast tissue have been shown to be ~68%,[43] and the tested range here was chosen as it is inclusive of saturation levels that meet or exceed those expected in human breast measurements. There is less than 5% disagreement in oxygen saturation measurements between the wearable probe and the DO sensor over this range, with an R^2 value of 0.998. Figure 5(b) shows changes in oxyhemoglobin (HbO_2), deoxyhemoglobin (HHb), and total hemoglobin (THb) over the 43-min period. There was reasonable agreement between the wearable probe and the DO sensor for HbO_2 changes, with a difference of 2.13 μM by the end of the test. There were slightly larger differences in HHb measurements, with a maximum difference of 2.84 μM by the end of the test. These differences may be caused by a number of factors, including errors in the initial optical property estimates or small system nonlinearities.

4 In Vivo Measurements

4.1 *Cuff Occlusion Test*

A cuff occlusion test was performed to demonstrate the *in vivo* measurement performance of the wearable probe. Baseline optical properties of the forearm were obtained from literature values.[44,45] The MBLL was used to determine chromophore concentration changes as before with optical scattering assumed constant over the measurement. Measurements were taken every 1.02 s during the occlusion test.

Figure 6 shows continuous extractions of oxyhemoglobin, deoxyhemoglobin, and total hemoglobin molar concentration changes from a single source–detector pair during the cuff occlusion. The wearable probe was securely attached to the forearm, and an adult blood pressure cuff was applied to the upper arm of a healthy volunteer with no pressure added to the aneroid sphygmomanometer. Starting from $t = 30$ s, cuff pressure was rapidly increased to a maximum of ~200 mmHg. From the 30th second to the 150th second, the concentration of oxyhemoglobin gradually decreased while deoxyhemoglobin concentration increased at a faster rate. Changes in the total hemoglobin concentration during this period indicate a net influx of oxygenated blood into the forearm, which might be due to incomplete occlusion of arterial supply. At $t = 150$ s, the cuff pressure was released, and oxygenated blood quickly refilled the forearm circulation, causing a rapid rise in oxyhemoglobin and total hemoglobin with a corresponding decrease in deoxyhemoglobin. Chromophore concentrations gradually returned to steady state. These observations match expectations and demonstrate the ability of the probe to measure hemodynamic changes in the *in vivo* setting.[46]

4.2 *Normal Volunteer Test*

As a proof of concept, a normal volunteer test was conducted on a 46-year-old premenopausal woman to evaluate the feasibility of taking continuous measurement over healthy female breast tissue. This test was carried out under the approval of Boston University Institutional Review Board.

The wearable probe was placed on the top left corner of her left breast, with a 5 mm distance between the wearable probe and the nipple. The HDMI cable was supported by placing it over the subject's neck and the wearable probe was secured using IV tape. The probe was allowed a 10 min warm-up and stabilization period prior to optical measurements. The volunteer was allowed to move in the chair during the measurement. Repeated measurement cycles were taken every 1.2 s.

Figure 7 shows chromophore concentration changes over a 10-min measurement period, which is a portion of a longer measurement. A 0.08-Hz low-pass filter was applied to remove

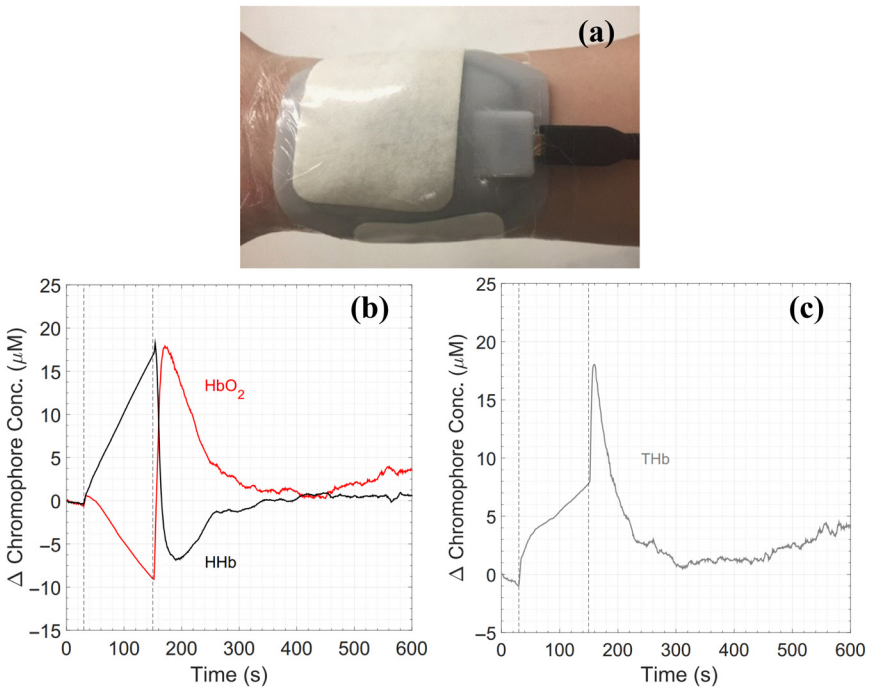

Fig. 6 (a) The probe is secured to the subject's skin using IV tape during cuff occlusion measurements. (b) and (c) Hemodynamic response at forearm during cuff occlusion test.

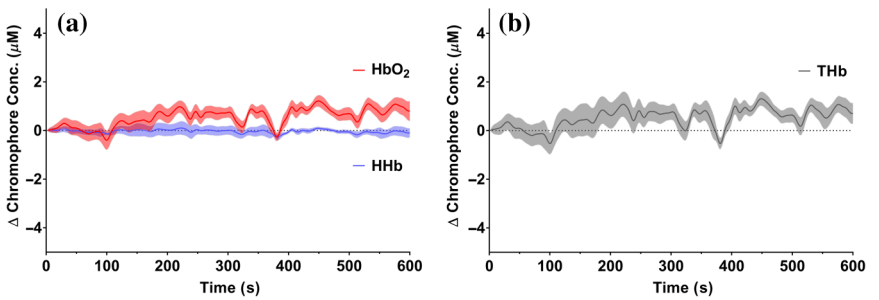

Fig. 7 Hemodynamic fluctuations of healthy female breast tissue at resting state. (a) Oxyhemoglobin (HbO_2) and deoxyhemoglobin (HHb); (b) total hemoglobin (THb).

known physiological signals including heart beat (~1 Hz, aliased to 0.17 Hz for the sampling rate used), respiration (0.2 to 0.3 Hz) and Mayer waves (~0.1 Hz).[47–49] The remaining low frequency components are expected to contain contributions from motion as well as tissue oxygenation fluctuations during resting state, which typically vary on subminute to minute time frames.[50] Prior to filtering, variations in CW signal level were generally around 5%, which agrees well with previously reported measurements on healthy breast tissue over a similar time frame.[36] We note that motion artifacts do have the potential to mask or mimic underlying physiological changes in breast tissue, and methods to detect and remove these from the data are currently being investigated.

5 Discussion

This work demonstrated the performance of a new, deep-tissue, optical wearable probe designed for monitoring breast cancer patients during presurgical chemotherapy. Tissue-simulating phantom measurements revealed low crosstalk (−60 dB), high SNR (71 dB), high precision (0.17%), and good thermal stability (0.22% V_{rms}/°C). The accuracy of our CW measurements was evaluated with a blood liquid phantom at different saturation levels, which resulted in less than 5% error in oxygen saturation estimates. Cuff occlusion and breast measurements reflected expected tissue hemodynamics.

The probe was specifically designed to monitor breast tumor oxygenation changes throughout chemotherapy infusions, which typically consist of one to three different cytotoxic and/or targeted agents sequentially infused intravenously of a period of several hours. There are several application-specific considerations that affected the design of this probe and ultimately differentiate it from other ambulatory and wearable diffuse optical devices that have been developed for monitoring cerebral or muscle oxygenation. First, the probe was designed to be highly flexible to conform to the natural breast tissue shape while still being housed in a single unit with static optode geometry in order to enable measurement comparisons between subjects. Additionally, although the investigation of chemotherapy-induced changes during infusions is an emerging area of research, it is expected that substantial hemodynamics will likely change over timescales of minutes to hours, substantially slower than the timecourse of cerebral evoked potential or

functional activations typically observed in the brain, or muscle contraction and relaxation observed for fitness monitoring applications. This relaxes the requirement for rapid measurement speeds often sought for other DOT applications but increases the need for stable and repeatable measurements over long time periods. Our design was shown to provide highly stable measurements during phantom experiments, and only small fluctuations were observed during the normal breast measurement, but the issue of motion artifact reduction must be properly addressed prior to implementation in the clinical setting. We are currently exploring better ways of stabilizing the probe on the breast along with signal processing approaches for removing these artifacts from the data. It is of note that the largest change from baseline in HbO_2 concentration observed during the normal volunteer measurements in this study was ~8% over a 10-min period. In comparison, changes of ~20% to 40% in HbO_2 were observed after the first 24 h in patients receiving neoadjuvant chemotherapy in a prior study.[20] In the future, a normal volunteer study will be conducted to better identify the magnitude of natural physiological variations in breast hemodynamics during multihour measurements in order to better understand how continuous measurements may be able to track treatment response.

To the best of our knowledge, this CW imaging system is the first demonstration of a wearable device aimed at continuously monitoring the hemodynamic response from breast cancer patients and represents a promising new tool to target unexplored prognostic timepoints during neoadjuvant chemotherapy infusions.

Disclosures

The authors have no conflicts of interest.

Acknowledgments

The authors gratefully acknowledge funding from the National Institute of Biomedical Imaging and Bioengineering of the National Institutes of Health (NIBIB-NIH) under Grant No. 5-U54-EB015403 and the Boston University—Fraunhofer USA Inc. Alliance Award.

References

1. S. L. Jacques and B. W. Pogue, "Tutorial on diffuse light transport," *J. Biomed. Opt.* **13**(4), 041302 (2008).
2. R. Choe and T. Durduran, "Diffuse optical monitoring of the neoadjuvant breast cancer therapy," *IEEE J. Sel. Top. Quantum Electron.* **18**(4), 1367–1386 (2012).
3. T. H. Pham et al., "Broad bandwidth frequency domain instrument for quantitative tissue optical spectroscopy," *Rev. Sci. Instrum.* **71**(6), 2500–2513 (2000).
4. B. Pogue et al., "Instrumentation and design of a frequency-domain diffuse optical tomography imager for breast cancer detection," *Opt. Express* **1**(13), 391 (1997).
5. G. Yu et al., "Frequency-domain multiplexing system for in vivo diffuse light measurements of rapid cerebral hemodynamics," *Appl. Opt.* **42**(16), 2931 (2003).
6. L. Gao et al., "Effects of assuming constant optical scattering on haemoglobin concentration measurements using NIRS during a Valsalva Manoeuvre," in *Oxygen Transport to Tissue XXXII*, pp. 15–20, J. C. LaManna et al., Eds., Springer, Unite States (2011).
7. S. M. Coyle, T. E. Ward, and C. M. Markham, "Brain-computer interface using a simplified functional near-infrared spectroscopy system," *J. Neural Eng.* **4**(3), 219–226 (2007).
8. P. B. Benni et al., "Validation of the CAS neonatal NIRS system by monitoring VV-ECMO patients," in *Oxygen Transport to Tissue XXVI*, pp. 195–201, P. Okunieff, J. Williams, and Y. Chen, Eds., Springer, United States (2005).
9. M. M. Tisdall et al., "The effect on cerebral tissue oxygenation index of changes in the concentrations of inspired oxygen and end-tidal carbon dioxide in healthy adult volunteers," *Anesth. Analg.* **109**(3), 906–913 (2009).
10. R. Stojanovic and D. Karadaglic, "Design of an oximeter based on LED-LED configuration and FPGA technology," *Sensors* **13**(1), 574–586 (2013).
11. T. Muehlemann, D. Haensse, and M. Wolf, "Wireless miniaturized in-vivo near infrared imaging," *Opt. Express* **16**(14), 10323 (2008).
12. S. K. Piper et al., "A wearable multi-channel fNIRS system for brain imaging in freely moving subjects," *Neuroimage* **85**(1), 64–71 (2014).
13. P. Pinti et al., "Using fiberless, wearable fNIRS to monitor brain activity in real-world cognitive tasks," *J. Vis. Exp. JoVE* **106** (2015).
14. H. Atsumori et al., "Development of wearable optical topography system for mapping the prefrontal cortex activation," *Rev. Sci. Instrum.* **80**(4), 43704 (2009).
15. R. McKendrick, R. Parasuraman, and H. Ayaz, "Wearable functional near infrared spectroscopy (fNIRS) and transcranial direct current stimulation (tDCS): expanding vistas for neurocognitive augmentation," *Front. Syst. Neurosci.* **27** (2015).
16. A. E. Cerussi et al., "Frequent optical imaging during breast cancer neoadjuvant chemotherapy reveals dynamic tumor physiology in an individual patient," *Acad. Radiol.* **17**(8), 1031–1039 (2010).
17. N. Shah et al., "Noninvasive functional optical spectroscopy of human breast tissue," *Proc. Natl. Acad. Sci.* **98**(8), 4420–4425 (2001).
18. S. Jiang et al., "Predicting breast tumor response to neoadjuvant chemotherapy with diffuse optical spectroscopic tomography prior to treatment," *Clin. Cancer Res.* **20**(23), 6006–6015 (2014).
19. C. Zhou et al., "Diffuse optical monitoring of blood flow and oxygenation in human breast cancer during early stages of neoadjuvant chemotherapy," *J. Biomed. Opt.* **12**(5), 051903 (2007).
20. D. Roblyer et al., "Optical imaging of breast cancer oxyhemoglobin flare correlates with neoadjuvant chemotherapy response one day after starting treatment," *Proc. Natl. Acad. Sci. U. S. A.* **108**(35), 14626–14631 (2011).
21. S. Ueda et al., "Baseline tumor oxygen saturation correlates with a pathologic complete response in breast cancer patients undergoing neoadjuvant chemotherapy," *Cancer Res.* **72**(17), 4318–4328 (2012).
22. O. Falou et al., "Diffuse optical spectroscopy evaluation of treatment response in women with locally advanced breast cancer receiving neoadjuvant chemotherapy," *Transl. Oncol.* **5**(4), 238–246 (2012).
23. P. Taroni et al., "Noninvasive assessment of breast cancer risk using time-resolved diffuse optical spectroscopy," *J. Biomed. Opt.* **15**(6), 060501 (2010).
24. L. Spinelli et al., "Characterization of female breast lesions from multi-wavelength time-resolved optical mammography," *Phys. Med. Biol.* **50**(11), 2489–2502 (2005).
25. A. Torricelli et al., "Use of a nonlinear perturbation approach for in vivo breast lesion characterization by multiwavelength time-resolved optical mammography," *Opt. Express* **11**(8), 853 (2003).
26. P. G. Anderson et al., "Broadband optical mammography: chromophore concentration and hemoglobin saturation contrast in breast cancer," *PloS One* **10**(3), e0117322 (2015).
27. M. L. Flexman et al., "Digital optical tomography system for dynamic breast imaging," *J. Biomed. Opt.* **16**(7), 076014 (2011).
28. M. L. Flexman et al., "Optical biomarkers for breast cancer derived from dynamic diffuse optical tomography," *J. Biomed. Opt.* **18**(9), 096012 (2013).
29. A. E. Cerussi et al., "Diffuse optical spectroscopic imaging correlates with final pathological response in breast cancer neoadjuvant chemotherapy," *Philos. Trans. R. Soc. Lond. Math. Phys. Eng. Sci.* **369**(1955), 4512–4530 (2011).
30. Q. Zhu et al., "Noninvasive monitoring of breast cancer during neoadjuvant chemotherapy using optical tomography with ultrasound localization," *Neoplasia* **10**(10), 1028–1040 (2008).
31. D. R. Busch et al., "Optical malignancy parameters for monitoring progression of breast cancer neoadjuvant chemotherapy," *Biomed. Opt. Express* **4**(1), 105–121 (2013).
32. H. Soliman et al., "Functional imaging using diffuse optical spectroscopy of neoadjuvant chemotherapy response in women with locally advanced breast cancer," *Clin. Cancer Res.* **16**(9), 2605–2614 (2010).

33. A. T. Eggebrecht et al., "Mapping distributed brain function and networks with diffuse optical tomography," *Nat. Photonics* **8**(6), 448–454 (2014).
34. A. Cerussi et al., "Predicting response to breast cancer neoadjuvant chemotherapy using diffuse optical spectroscopy," *Proc. Natl. Acad. Sci.* **104**(10), 4014–4019 (2007).
35. M. Izzetoglu et al., "Functional near-infrared neuroimaging," *IEEE Trans. Neural Syst. Rehabil. Eng.* **13**(2), 153–159 (2005).
36. T. Durduran et al., "Bulk optical properties of healthy female breast tissue," *Phys. Med. Biol.* **47**(16), 2847–2861 (2002).
37. N. Shah et al., "Spatial variations in optical and physiological properties of healthy breast tissue," *J. Biomed. Opt.* **9**(3), 534–540 (2004).
38. B. Olesen, "Thermal comfort," *Tech. Rev.* **11**, 3–37 (1982).
39. G. R. Kelman, "Digital computer subroutine for the conversion of oxygen tension into saturation," *J. Appl. Physiol.* **21**(4), 1375–1376 (1966).
40. L. Kocsis, P. Herman, and A. Eke, "The modified Beer-Lambert law revisited," *Phys. Med. Biol.* **51**(5), N91 (2006).
41. S. R. Arridge, M. Cope, and D. T. Delpy, "The theoretical basis for the determination of optical pathlengths in tissue: temporal and frequency analysis," *Phys. Med. Biol.* **37**(7), 1531–1560 (1992).
42. C. M. Fraser, *The Merck Veterinary Manual: A Handbook of Diagnosis, Therapy, and Disease Prevention and Control for the Veterinarian*, Merck & Company (1991).
43. S. Srinivasan et al., "In vivo hemoglobin and water concentrations, oxygen saturation, and scattering estimates from near-infrared breast tomography using spectral reconstruction," *Acad. Radiol.* **13**(2), 195–202 (2006).
44. M.-A. Franceschini et al., "Near-infrared absorption and scattering spectra of tissues in vivo," *Proc. SPIE* **3597**, 526–531 (1999).
45. S. J. Matcher, M. Cope, and D. T. Delpy, "In vivo measurements of the wavelength dependence of tissue-scattering coefficients between 760 and 900 nm measured with time-resolved spectroscopy," *Appl. Opt.* **36**(1), 386 (1997).
46. T. Li et al., "Simultaneous measurement of deep tissue blood flow and oxygenation using noncontact diffuse correlation spectroscopy flow-oximeter," *Sci. Rep.* **3**, 1358 (2013).
47. V. Toronov et al., "Near-infrared study of fluctuations in cerebral hemodynamics during rest and motor stimulation: temporal analysis and spatial mapping," *Med. Phys.* **27**(4), 801–815 (2000).
48. E. Kirilina et al., "Identifying and quantifying main components of physiological noise in functional near infrared spectroscopy on the prefrontal cortex," *Front. Hum. Neurosci.* **7** (2013).
49. Y. Tong, K. P. Lindsey, and B. deB Frederick, "Partitioning of physiological noise signals in the brain with concurrent near-infrared spectroscopy and fMRI," *J. Cereb. Blood Flow Metab.* **31**(12), 2352–2362 (2011).
50. S. Jiang et al., "Pilot study assessment of dynamic vascular changes in breast cancer with near-infrared tomography from prospectively targeted manipulations of inspired end-tidal partial pressure of oxygen and carbon dioxide," *J. Biomed. Opt.* **18**(7), 076011 (2013).

Biographies for the authors are not available.